ICEMG 2019-XXXXX

Numerical Investigation of Axial Fan Blades Geometry on Induction electrical Motors

Hadi Marouf[1], Morteza Galian Rostami[2]

[1]M.Sc. in Mechanical Engineering, Jovain Electrical Machines Industries Company (JEMCO), Sabzevar, hadi.maroof@gmail.com
[2]P.hD. candidate in Mechanical Engineering, Jovain Electrical Machines Industries Company (JEMCO), Sabzevar, mrostami3015@gmail.com

Abstract
One of the essential parameters in designing electrical motors is heat generation by the motor and the way it is dissipated. Temperature rising reduces efficiency and reliability of induction electrical motors and leads to failure. In this paper, a case study for axial fan blades by using the theory of computational fluid dynamics (CFD) has been investigated. The axial fan is designed, manufactured and tested in Jovain Electrical Machines Industries Company (JEMCO) for a 2000 Kw induction electrical motors with the international cooling IC616 (according to the Std. IEC60034-6) and the insulation class B, which means the maximum ambient temperature is 40 °C and permissible temperature rise up to maximum 120 °C (according to the Std. IEC60034-1). In the mentioned electrical motor, air is blown directly from atmosphere into the heat exchanger that is assembled above the electrical motor and discharged to the atmosphere after passing through the pipes of heat exchanger; on the other hand, one internal air circulation for transport the generated heat of electrical motor to heat exchanger by one centrifugal fan is used. Six types of blades are designed and simulated to peruse some parameters such as velocity, turbulence parameters, pressure and shear stress on blades and inside connection cylinder. The CFD analyses show that axial fans with gradient blades and fans with cylindrical fins on above surface of blades improve the performance.

Keywords: induction electrical motor, heat generation, axial fan performance, computational fluid dynamics.

Introduction

An induction motor or asynchronous motor is an AC electrical motor in which the electric current in the rotor needed to produce torque is obtained by electromagnetic induction from the magnetic field of the stator winding[1]. An induction electrical motor can therefore be made without electrical connections to the rotor. An induction motor's rotor can be either wound type or squirrel-cage type. Three phase squirrel-cage induction motors are widely used as industrial drives because they are self-starting, reliable and economical. In this kind of electrical motor, the operating temperature has direct effects on the efficiency, lifetime and breakdown of electrical motors. For example, coil electrical resistance enhances when the operating temperature of the electrical motor raises which results to decrease the efficiency. In recent years due to developments of finite element method and computational fluid dynamics, application of these methods to analyze the performance of electrical machines has increased that some of them will be pointed in the following.

Nezih Gokhan Ozcelik et al. [2] studied on various kinds of electrical motors and concluded that increasing the stack length would be a suitable solution to increase the efficiency by decreasing voltage levels. Moayedirad et al. [3] presented a method based on rotor flux compensation for reducing the power losses of the inverter unit in the squirrel-cage dual stator induction motor drive with dissimilar numbers of pole at low speeds to increase electrical motors efficiency. Salomon et al. [4] introduced a mathematical AGT-based model for induction electrical motor torque and efficiency estimation experimentally. Xia et al. [5] proposed a 3D transient model to obtain the transient temperature distribution of motor in starting process under different loads but they do not investigated about the efficiency. One of the important factors to improve the induction electrical motors is cooling system, and the fan have an essential rule on performance of cooling system. Many authors have studied on fan geometry that mentioned in the following.

Yujing et al. [6] examined three design options (straight blades, C-type blades and forward swept blades) on their paper. They observed that the total pressure efficiency of the axial flow fan with the forward swept blade is the highest. Hasan koten [7] investigated the performance of a 16-blade axial fan and analyzed in 3D using computational fluid dynamic (CFD) technique, but he didn't use other blade numbers on his study. Fenner and Watson [8] investigated the fan to predict the stress, strain and vibrations modes of fan blades. Damian and Paleu [9] studied on exhaust fan with MSC/NASTRAN® to show differences between welded blades and bolted blades. Also, Wu et al. [10] investigated the effect of attack angle on flow characteristic of centrifugal fan. Effects of blades number on fan performance are studied by Adeeb et al. [11]. In addition, CFD, numerical and experimental techniques have been used to improve airflow and energy efficiency on fans (Hsieh, Rizk et al., Momoi et al., Sathaye et al. and Lubliner et al. [12-16].

This paper is a part of national technology transfer project of induction electrical motor propulsion system design for supply and transport agriculture necessary water from Aras Dam Lake to Karamabad dam. In this survey, a case study for axial fan blades by using computational fluid dynamics (CFD) has been investigated. The axial fan is designed, manufactured and tested in Jovain Electrical Machines Industries Company (JEMCO) for a 2000 Kw induction electrical motors. Six types of specific axial fan blades are simulated and analyzed dynamically and velocity, turbulence parameters and etc. compared entirely.

Simulation Details

Computational Domain

A computational fluid dynamic analysis usually has being used in these cases. We use Solid Works/ COSMOS simulation program to predict the average velocity, shear stress, pressure and turbulence parameters on the fan and the connection cylinder between the fan and the heat exchanger. The components that have any influence on the fluid flow path and heat transfer are considered. The manufactured induction electrical motor on JEMCO is shown in "Figure 1".

A ten-blades fan is simulated in six various ways and other geometrical parameters in electrical motor are same in all kinds. "Figure 2" demonstrates all kinds of blades (B_1 to B_6), the basic blade B_1, is made of two different airfoils at the bottom and top of the blade "Table 1". Blade B_2 has same airfoils as blade B_1 with seven rectangular grooves (4mm width and 2mm depth). The airfoils data of the third blade, gradient blade, (B_3) is inserted in "Table 2". Airfoils of blade B_4 is similar to blade B_1 with scale factor of 1.2. Blades B_5 and B_6 are similar to the blade B_1 with ninety two cylindrical (3mm diameter and 5mm height) and seven rectangular fins (4mm width and 5mm height) on the above surface respectively, The height of all blades is 100 mm. "Figure 3" shows the schematics of the basic axial fan.

Figure 1. The JEMCO induction electrical motor-2000Kw

Boundary Condition

At inlet, air is blown from ambient with temperature of 40°C. So a boundary condition with atmospheric pressure was applied to inlet of the computational domain. In the entrance of heat exchanger, there is an axial fan that creates a pressure drop causes the intake air flows to around the motor components, then air directly discharges to atmosphere. Connection cylinder amused as real walls and air as only fluid considered fully developed.

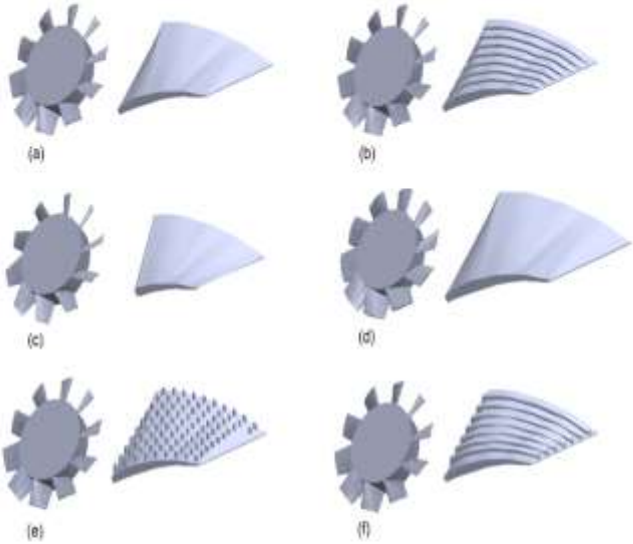

Figure 2. The six fan blade types, (a) Blade B_1. (b) Blade B_2. (c) Blade B_3. (d) Blade B_4. (e) Blade B_5. (f) Blade B_6

Table 1. Airfoils data of blades B_1, B_2, B_5 and B_6

Lower airfoil data		Upper airfoil data	
0,2882E+1	0,8718E+1	0,1218E+2	0,4526E-1
0,6068E+0	0,1100E+2	0,1020E+2	0,1409E+1
0,1061E+1	0,1406E+2	0,9909E+1	0,3695E+1
0,1077E+2	0,1713E+2	0,1174E+2	0,5378E+1
0,2503E+2	0,2067E+2	0,1907E+2	0,1180E+2
0,3625E+2	0,2175E+2	0,2624E+2	0,1686E+2
0,5309E+2	0,2193E+2	0,3463E+2	0,2071E+2
0,6887E+2	0,2103E+2	0,4271E+2	0,2470E+2
0,7812E+2	0,1982E+2	0,5079E+2	0,2824E+2
0,8996E+2	0,1815E+2	0,5918E+2	0,3116E+2
0,9997E+2	0,1526E+2	0,6786E+2	0,3287E+2
0,1087E+3	0,1267E+2	0,7701E+2	0,3596E+2
0,1081E+3	0,1145E+2	0,8493E+2	0,3706E+2
0,1010E+3	0,1174E+2	0,9574E+2	0,3786E+2
0,8981E+2	0,1372E+2	0,9574E+2	0,3664E+2
0,7084E+2	0,1538E+2	0,8340E+2	0,3370E+2
0,5689E+2	0,1536E+2	0,6907E+2	0,2937E+2
0,3944E+2	0,1350E+2	0,5474E+2	0,2383E+2
0,2457E+2	0,1211E+2	0,4071E+2	0,1676E+2
0,1243E+2	0,1041E+2	0,2804E+2	0,9556E+1

Table 2. Airfoils data of blade B_3

Lower airfoil data		Upper airfoil data	
0,2882E+1	0,8718E+1	0,3471E+2	0,1753E+2
0,6068E+0	0,1100E+2	0,3503E+2	0,1966E+2
0,1061E+1	0,1406E+2	0,3626E+2	0,2149E+2
0,1077E+2	0,1713E+2	0,3978E+2	0,2271E+2
0,2503E+2	0,2067E+2	0,4437E+2	0,2484E+2
0,3625E+2	0,2175E+2	0,4727E+2	0,2667E+2
0,5309E+2	0,2193E+2	0,5430E+2	0,2926E+2
0,6887E+2	0,2103E+2	0,6041E+2	0,3125E+2
0,7812E+2	0,1982E+2	0,6530E+2	0,3231E+2
0,8996E+2	0,1815E+2	0,6881E+2	0,3323E+2
0,9997E+2	0,1526E+2	0,7889E+2	0,3582E+2
0,1087E+3	0,1267E+2	0,8667E+2	0,3628E+2
0,1081E+3	0,1145E+2	0,9537E+2	0,3780E+2
0,1010E+3	0,1174E+2	0,9629E+2	0,3765E+2
0,8981E+2	0,1372E+2	0,9628E+2	0,3628E+2
0,7084E+2	0,1538E+2	0,8513E+2	0,3338E+2
0,5689E+2	0,1536E+2	0,7582E+2	0,3155E+2
0,3944E+2	0,1350E+2	0,6344E+2	0,2652E+2
0,2457E+2	0,1211E+2	0,4891E+2	0,2012E+2
0,1243E+2	0,1041E+2	0,3836E+2	0,1509E+2

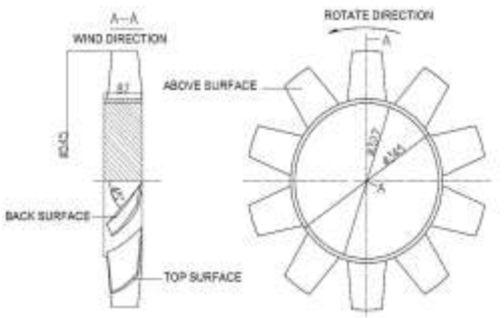

Figure 3. The basic axial fan schematics.

Solution Method

Due to the Reynolds number, much of the fluid regime in practical condition is turbulent; the surrounding around the induction electrical motors fan is turbulent too. Turbulent kinetic energy is one of the essential equations that demonstrated with (K), which often used from "Equation 1":

$$K = \frac{1}{2}(\bar{u}_i'\bar{u}_j') = \frac{1}{2}(u'^2 + v'^2 + w'^2) \quad (1)$$

The Reynolds stress term has been accrued from $\bar{u}_i'\bar{u}_j'$ that approximated by turbulent viscose. "Equation 2" demonstrates Boussinesq model.

$$-\rho < \bar{u}_i'\bar{u}_j' >= 2\mu_t S_{ij} - \frac{2}{3}\rho K \delta_{ij} \quad (2)$$

Where $\bar{u}_i'\bar{u}_j'$ is the Reynolds stress, μ_t is the turbulence viscose and K is the average fluid turbulence energy.

$$\mu_t = Const.\rho K^{\frac{1}{2}} L \quad (3)$$

Where L is mixing length.

Product of oscillating viscose stresses that is produced from viscose diffusion in fluid oscillating strain field generates turbulence dissipation.

$$\epsilon = \nu \frac{\partial u_i'}{\partial x_k}\frac{\partial u_i'}{\partial x_k} \quad (4)$$

That by using the dimensional agronomics analysis turbulence dissipation approximated with "Equation 5".

$$\epsilon \sim \frac{K^{\frac{3}{2}}}{L} \quad (5)$$

Result and Discussion

In this optimization study, mesh geometry, the variation of turbulent parameters, pressure, shear stress and velocity along the axial fan and along the slope of the case were investigated. Quad elements were used as a mesh element. Since cases examined during the study, the mesh sizes of the models were predicted in "Table 3". Boundary conditions were defined in commercial CFD code. At the fan sidewalls, constant temperature was assumed. Connection cylinder material was defined as steel (St37-2). At the air inlet, standard atmospheric conditions were defined as the boundary condition. Also the total computational time for the grid use of all blades according to the CPU time on the HP DL380 G7 with 32 GB of RAM is shown in this table.

Table 3. Grid system and CPU time for all blades

	Fluid Cells	Solid Cells	Total Cells	CPU Time (min)
B_1	416782	284807	701589	44
B_2	1025111	835132	1860243	135
B_3	1292036	921991	2214027	188
B_4	1014221	743600	1757821	132
B_5	1036959	788656	1825615	134
B_6	3298011	2987030	6285041	628

For all six axial fans inlet volume flow is 5 m^3/s and fans rotate in 1500 rpm. Results of all simulation are compared with each other to investigate which one is more appropriate in special cases. Average values for some goal parameters are inserted in "Table 4". The blades B_4 and B_6 provide higher pressure in comparison with other blades and blade B_3 provides higher velocity on the connection cylinder. Blade B_5 has the lowest turbulence among all blades. So, it provides the lowest shear stress.

"Figure 4" shows the velocity vector on the above surface of all six blades. The average velocity on the above surface in blade B_3 with 99.590 (m/s) is the highest one and in blades B_4, B_5, B_6, B_2 and B_1 is 94.833 (m/s), 94.048 (m/s), 94.022 (m/s), 87.122 (m/s) and 71.991 (m/s) respectively. "Figure 5" predicts two-dimensional air flow velocity in the connection cylinder. The average velocity on back and top surfaces of all six blades are inserted in "Table 5".

The velocity and turbulence length of flow trajectories for all six blades are shown in "Figure. 6" and "Figure 7". The maximum velocity and turbulence length are 30 (m/s) and 0.005 (m) respectively. "Figure 8" shows the air flow trajectories velocity on a blade in all six axial fans three- dimensionally.

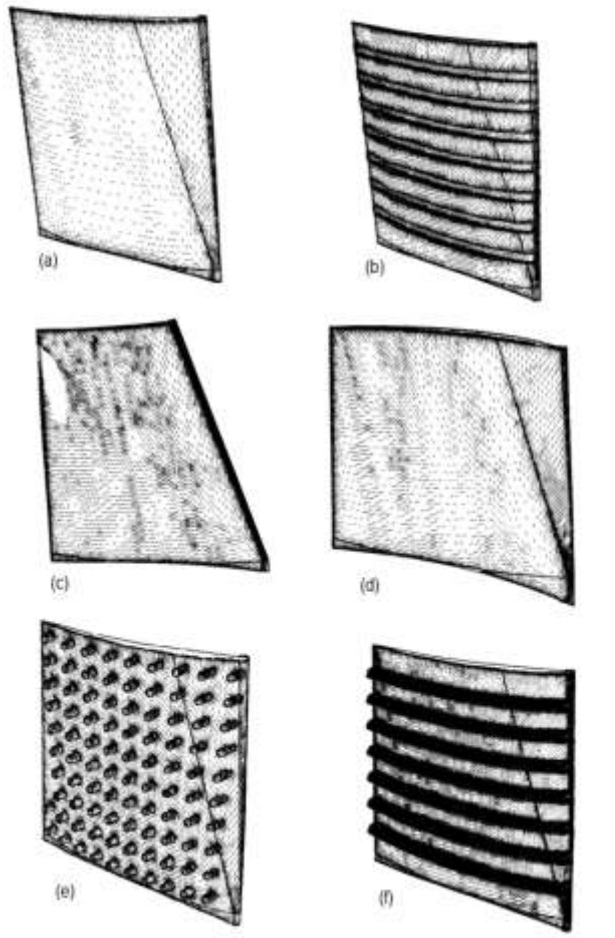

Figure 4. Velocity vectors on above surface, (a) Blade B_1. (b) Blade B_2. (c) Blade B_3. (d) Blade B_4. (e) Blade B_5. (f) Blade B_6

Table 4. Goal parameters

	Average Value					
Name	B_1	B_2	B_3	B_4	B_5	B_6
P_S (KPa)	101.391	101.391	101.390	101.394	101.392	101.394
P_T (KPa)	101.495	101.495	101.495	101.499	101.492	101.498
P_D (Pa)	103.22	104.06	105.02	104.62	99.52	103.41
V (m/s)	10.741	10.827	11.002	10.927	10.484	10.791
S (Pa.s)	16e-4	15e-4	0.228	4e-4	5e-4	4e-4
T (s)	0.172	0.165	0.192	0.210	0.215	0.237
l (m)	0.002	0.002	0.002	0.001	0.0006	0.001
I (%)	6.37	5.61	4.66	3.68	2.94	3.74
K (J/kg)	0.878	0.795	0.432	0.280	0.055	0.260
ϵ (W/kg)	160.22	157.27	73.68	65.67	25.26	107.39
ζ (Pa)	2.61	2.68	1.98	2.24	1.97	2.30

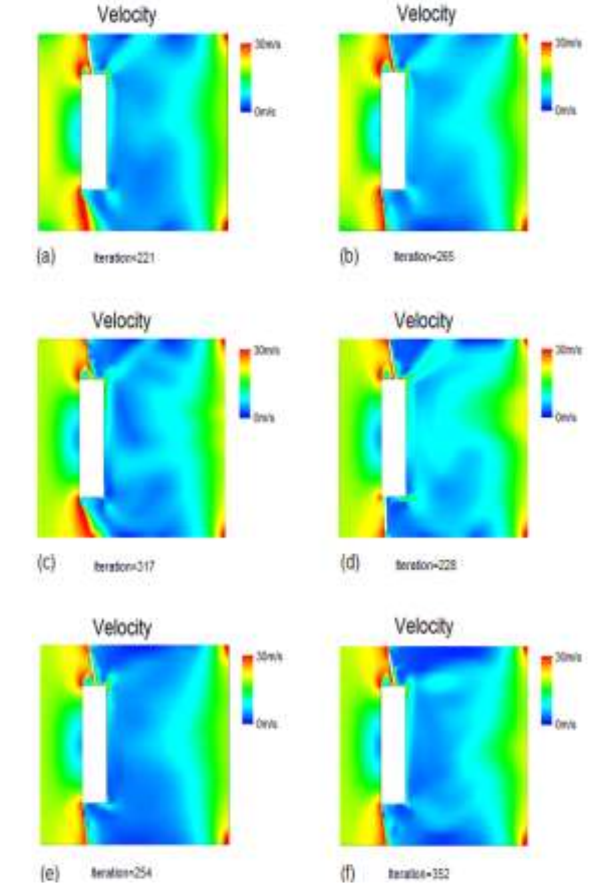

Figure 5. Two- dimensional air flow velocity in connection cylinder, (a) Blade B_1. (b) Blade B_2. (c) Blade B_3. (d) Blade B_4. (e) Blade B_5. (f) Blade B_6

Table 5. Average velocity on back and top surfaces

Name	Back Surface Average Velocity (m/s)	Top Surface Average Velocity (m/s)
B_1	88.082	93.937
B_2	86.921	92.566
B_3	87.460	100.440
B_4	94.766	102.286
B_5	94.766	101.456
B_6	94.060	101.454

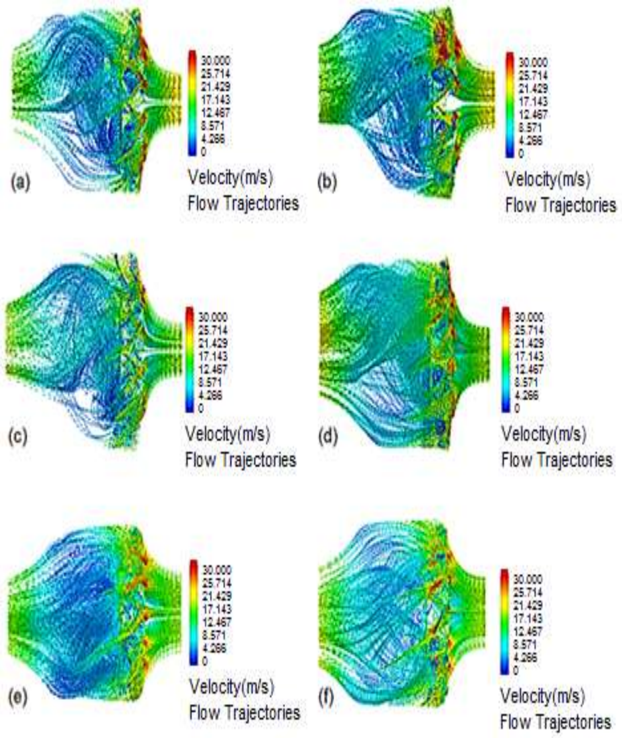

Figure 6. The velocity of air flow trajectories, (a) Blade B_1. (b) Blade B_2. (c) Blade B_3. (d) Blade B_4. (e) Blade B_5. (f) Blade B_6

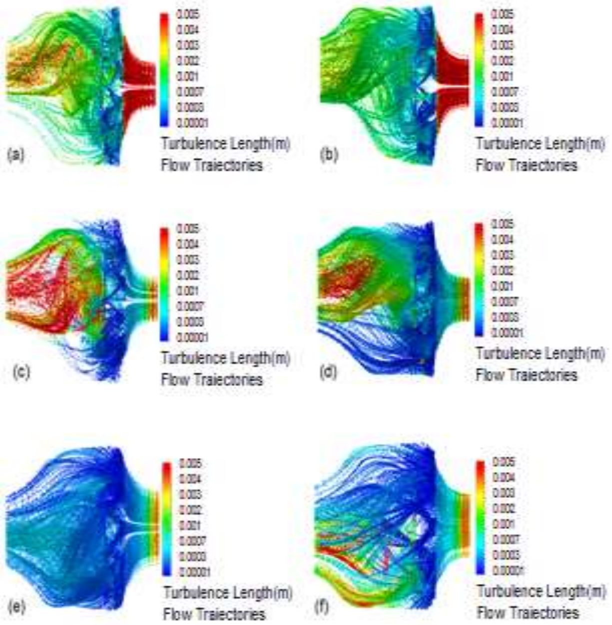

Figure 7. The turbulence length of air flow trajectories, (a) Blade B_1. (b) Blade B_2. (c) Blade B_3. (d) Blade B_4. (e) BladeB_5. (f) Blade B_6

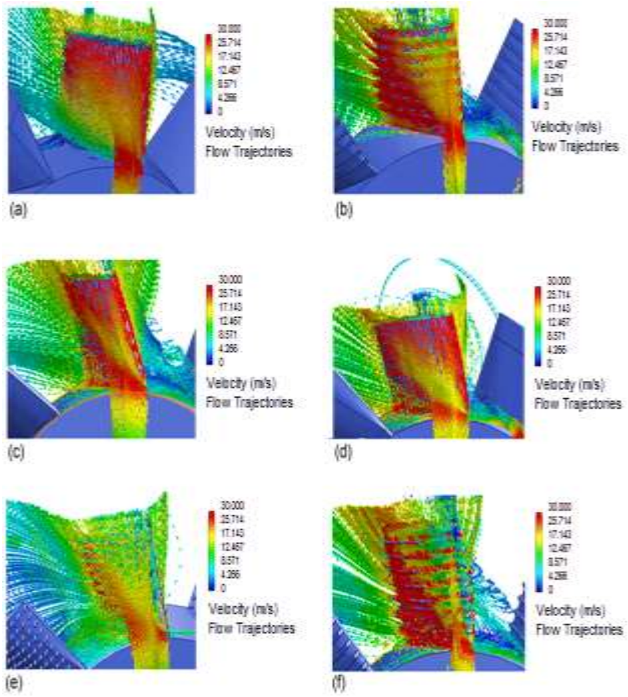

Figure 8. The 3D velocity of air flow trajectories, (a) Blade B_1. (b) Blade B_2. (c) Blade B_3. (d) Blade B_4. (e) Blade B_5. (f) Blade B_6

CONCLUSION

According to using the base blades in designing of produced induction electrical motor in JEMCO Company, 96.29% for efficiency is gained, now to investigate and analyze the reducing electrical motor temperature that raises the total efficiency, five other blades are designed and simulated which the results are adduced in the follow:

-Axial fan with cylindrical fins on above surface of blades (blade B_5) provides the most steady air flow in connection cylinder. Also produces the lowest air flow turbulence intensity, 53.85% decrement, and 93.73% decrease in turbulent energy in comparison with basic axial fan (blade B_1).

-Axial fan with gradient blades (blade B_3) and cylindrical fins on above surface of blades (blade B_5) provide about 24.52% diminution in shear stress in comparison with basic axial fan (blade B_1).

-Dynamic pressure has its lowest value in axial fan with cylindrical fins on above surface of blades (blade B_5), 3.58% lower than basic axial fan (blade B_1).

-The velocity of air flow in the outer part of connection cylinder is steadier than other parts in all cases.

-The maximum average velocity on top and back surfaces belongs to axial fan with blades with scale factor equals to 1.2(blade B_4), 8.16% and 7.05% enhance in compression with basic axial fan (blade B_1).

-Axial fan with gradient blades (blade B_3) provides the higher average velocity in connection cylinder, 2.37% increase in comparison with basic axial fan (blade B_1).

ACKNOWLEDGEMENTS

This work was supported by the Jovain Electrical Machines Industries Company (JEMCO). The authors thank to Mr. Mohammad Rostami, JEMCO CEO, who support this study technically.

NOMENCLATURE

B	blade	P_T	total pressure
I	turbulence intensity	μ_t	turbulent viscosity
K	turbulent energy	T	turbulent time
l	turbulence length	V	average velocity
P_D	dynamic pressure	ϵ	turbulent dissipation
P_S	static pressure	ζ	shear stress

References

[1] IEC 60050 (Publication date: 1990-10). Section 411-31: Rotation Machinery - General, IEV ref. 411-31-10: "Induction Machine - an asynchronous machine of which only one winding is energized"

[2] Ozcelik, N.G., Dogru, U.E., Imeryuz, M., and Ergene L.T., 2019. "Synchronous Reluctance Motor vs. Induction Motor at Low-Power Industrial Applications: Design and Comparison" .*Energies*, 12(11):2190, jun, pp. 1-20.

[3] Moayedirad, H., and Shamsi Nejad M.A., 2018. "Increasing the Efficiency of the Power Electronic Converter for a Proposed Dual Stator Winding Squirrel-Cage Induction Motor Drive Using a Five-Leg Inverter at Low Speeds". *Journal of Operation and Automation in Power Engineering*, 6(1), jun, pp. 23-39.

[4] Salomon, C.P., Sant'Ana, W.C., Borges da Silva, L.E., Lambert-Torres, G., Bonaldi, E.L., de Oliveira, L.E.L., and Borges da Silva, J.G., 2015. "Induction Motor Efficiency Evaluation Using a New Concept of Stator Resistance". *IEEE*, 64(11), Nov, pp. 2908-2917.

[5] Xia, Y., Xu, Y., Ai, M., and Liu, J., 2019. "Temperature Calculation of an Induction Motor in the Starting Process". *IEEE*, 29(2), Mar, pp. 1-4.

[6] Yujing, W.U., and Hung, D., 2019. "Optimization design of axial fan blade". *Journal of the Chinese Institute of Engineers*, 42(6), March, pp. 473-478.

[7] Koten, H., 2018. "CFD modeling and multi-objective optimization of the axial fan parameters". *Journal of Energy Systems*, 2(4), December, pp. 137-144.

[8] Fenner, P.E., and Watson, A., 2012. "Finite element buckling analysis of stiffened plates with filleted junctions". Thin-Walled Structures, 59, Oct, pp. 171-180.

[9] Damian, I. and V. Paleu., 2016. *7th International Conference on Advanced Concepts in Mechanical Engineering*, Materials Science and Engineering, 147, Nov, pp. 1-6.

[10] Wu, Y., Dou, H.S., Wei, Y.K., Chen, X.P., Chen, Y.N., and Cao, W.B., 2016. "Effect of attack angle on flow characteristic of centrifugal fan". *Materials Science and Engineering*, 129, pp. 1-21

[11] Adeeb, E., A. Maqsood and A. Mushtaq 2015, "Effect of Number of Blades on Performance of Ceiling Fans". MATEC Web of Conferences, 28, Jul, pp. 1-4.

[12] Hsieh, M.Y., 2014. "An Integrated Numerical and Experimental Analysis for Enhancing the Performance of the Hidden Ceiling Fan". *Advances in Mechanical Engineering*, 1, Feb, pp. 1-15.

[13] Rizk, A., EL-Deberky, A., and Guirguis, N., 2014. "Simulation comparison between natural and hybrid ventilation by fans at night time for severe hot climate". *Renewable Energy in the Service of Mankind*, 1, Feb, pp. 602-609.

[14] Momoi, Y., K. Sagara, T., Yamanaka, and H., Kotani, 2007. "Modeling of Ceiling Fan Based on Velocity Measurement for CFD Simulation of Airflow in Large Room". International Journal of Ventilation 1(1).

[15] Sathaye N., Phadke A., Shah N., and Letschert V., 2013. "Potential Global Benefits of Improved Ceiling Fan Energy Efficiency". *In ernest orlando lawrence berkeley national laboratory*, April, USA.

[16] Lubliner, M., J. Douglass, P.D. Parker, D. Chaser and PE, 2004. "Performance and applications of gossamer wind™ solar powered ceiling fans". *Florida Solar Energy Center*, September, USA.